

Discovery of a long thermonuclear X-ray burst from the ultra-compact binary 4U 1850–087YONGQI LU,¹ ZHAOSHENG LI,¹ WENHUI YU,¹ YUANYUE PAN,¹ AND MAURIZIO FALANGA^{2,3}¹*Key Laboratory of Stars and Interstellar Medium, Xiangtan University, Xiangtan 411105, Hunan, P.R. China*²*International Space Science Institute (ISSI), Hallerstrasse 6, 3012 Bern, Switzerland*³*Physikalisches Institut, University of Bern, Sidlerstrasse 5, 3012 Bern, Switzerland***ABSTRACT**

We report the detection of a long X-ray burst triggered on MJD 60171.65 from the ultra-compact binary 4U 1850–087 by the Monitor of All-sky X-ray Image and Neutron Star Interior Composition Explorer (*NICER*). We analyse the *NICER* data observed in between MJD 60095.19–60177.43, including one observation covered part of the long X-ray burst tail, i.e., 0.15–3.8 hr after the trigger. The persistent spectra are quite similar and well described by a combination of multi-color disk blackbody, with the inner temperature of 0.5 keV, and a thermally comptonized continuum with the asymptotic power-law photon index of $\Gamma \sim 2.2$, and electron temperature of $kT_e \sim 20 - 30$ keV. The persistent fluxes were around 3.8×10^{-10} erg cm⁻² s⁻¹, corresponding to a local accretion rate of 1% \dot{m}_{Edd} . Part of time-resolved burst spectra show a clear deviation from the blackbody model, which can be improved by considering the enhanced persistent emission due to the Poynting-Robertson drag, or the reflected disk emission illuminated by the burst. From the burst flux during the cooling tail, we estimate the burst duration, $\tau \approx 0.78$ hr, the burst fluence, $E_b \approx 4.1 \times 10^{41}$ ergs, and the ignition column depth, $y_{\text{ign}} \approx 3.5 \times 10^{10}$ g cm⁻². We propose that the long X-ray burst is powered by unstable burning of pure helium in deep layer. Moreover, we identify significant 1 keV emission lines in the burst spectra, which may originate from the surrounding disk.

1. INTRODUCTION

In a neutron star low-mass X-ray binary (NS LMXB), NS accretes matter from its companion star ($M < 1M_{\odot}$) through the Roche-lobe overflow, behaving as a persistent or transient source (Lasota 2001). The accreted matter, mainly composed of helium or mixed of hydrogen and helium, can be consumed through stable, marginally stable or unstable burning, which depends on the accretion rate and the abundance (Keek et al. 2012; Li et al. 2021). The unstable thermonuclear burning is also known as type I X-ray burst (hereafter X-ray burst, see Strohmayer & Bildsten 2006; Galloway & Keek 2021). X-ray bursts usually release total energy about 10^{39} erg and ignite at a typical column depth of $y_{\text{ign}} \sim 10^8$ g cm⁻². It lasts ~ 10 –100 s, depending on the thickness of the burning layer (see Lewin et al. 1993; Galloway et al. 2008; Galloway et al. 2020). Intermediate-duration bursts can release $\sim 10^{41}$ erg in

a longer duration of ~ 100 –1000 s and are powered by the unstable burning of helium in deep layer at an ignition column depth of $y_{\text{ign}} \sim 10^{10}$ g cm⁻² (see in’t Zand et al. 2005; Cumming et al. 2006; Falanga et al. 2008; Keek et al. 2010). Most intermediate-duration bursts occurred in the low accretion rate, that is lower than 1% of the Eddington limit (Falanga et al. 2008; Alizai et al. 2023). Superbursts have the longest duration of $> 10^3$ s and releasing energies of $\sim 10^{42}$ erg, which are powered by the unstable burning of carbon for its mass fraction reaching 15–30% (Cumming & Bildsten 2001; Strohmayer & Brown 2002). However, the X-ray bursts in 4U 0614+091 and SAX J1712.6–3739 with duration of hours were classified as intermediate-duration bursts since the accretion rates were around 1% of the local Eddington limit and cannot produce carbon sufficiently (see e.g., Kuulkers et al. 2010; in’t Zand et al. 2019; Alizai et al. 2023).

Several types of spectral features have been identified during X-ray bursts. The 1 keV emission lines have been observed in IGR J17062–6143 (Degenaar et al. 2013; Keek et al. 2017; Bult et al. 2021a) and SAX J1808.4–

3658 (Bult et al. 2021b), which were interpreted as a reflection feature from accretion disk, possibly associated with Fe-L band transitions. The 1 keV emission line was also observed in the bursts from 4U 1820–30 during the expansion phase (Strohmayer et al. 2019). The reflection features were observed in normal or long X-ray bursts (Strohmayer & Brown 2002; Ballantyne & Strohmayer 2004; Keek et al. 2014; Zhao et al. 2022; Lu et al. 2023).

4U 1850–087 is a persistent X-ray source, which was first detected as an X-ray burster by Swank et al. (1976) and immediately confirmed that the compact star is an NS. The possible 20.6 min orbital period of 4U 1850–087 suggested it belongs to an ultracompact X-ray binary (UCXB; Homer et al. 1996). 4U1850–087 is located in the globular cluster NGC 6712 at a distance of 8 kpc (Tremou et al. 2018). The *XMM-Newton* spectra showed clear O K, Fe L, and Ne K edges at 0.54, 0.71, and 0.87 keV, respectively (Sidoli et al. 2005). Several long X-ray bursts in 4U 1850–087 were detected by the Monitor of All-sky X-ray Image (*MAXI*) and *Swift* which have been suggested as the power of unstable burning of pure helium in deep layer due to their relatively high peak fluxes and low accretion rates (e.g., in’t Zand et al. 2014; Serino et al. 2016).

In this work, we analyze a long X-ray burst detected by *MAXI* and *NICER* in 2023 August 15. In Section 2, we introduce the observations and describe the properties of the persistent emissions and long X-ray burst. In Section 3, we perform the spectra fitting for the persistent and time-resolved burst emissions. We discuss the results in Section 4.

2. OBSERVATION AND DATA REDUCTION

MAXI and *NICER* are two instruments installed onboard the International Space Station on 2009 July 15 and 2017 June 3, respectively. *MAXI* performs a full-sky survey every 96 minutes, which can monitor the X-ray sources activities, e.g., X-ray outbursts and X-ray bursts. From the *MAXI* novae webpage¹, we noticed a long X-ray burst from 4U 1850–087 triggered on 2023 August 15 (MJD 60171.654514). We then cross-checked the archived data from *NICER*, and found six contemporaneous observations, including Obs. IDs 6617010101–6617010103 and 6403520101–6403520103 with the net unfiltered exposure time of 44 ks. The Obs. ID 6403520101 started on MJD 60171.66085, 0.15 hrs af-

ter the trigger of *MAXI*, partially covering the cooling tail of the long X-ray burst.

We used HEASOFT V6.31.1 and the *NICER* Data Analysis Software (NICERDAS) to process the *NICER* data. The standard filtering criteria have been applied, i.e., the pointing offset $< 54''$, the Earth elevation angle $> 15^\circ$, the elevation angle with respect to the bright Earth limb $\leq 30^\circ$, and the instrument locating outside the South Atlantic Anomaly (SAA). We used `nicerl3-1c` to extract the light curves in 0.5–10, 0.5–2, and 2–10 keV. The 64 s light curves in the energy range 0.5–10 keV are shown in Figure 1. To have better coverage of the data between MJD 60171–60172, we added the 2–20 keV light curves with 1 day binned from *MAXI*/GSC² in Figure 1.

We show the 64 s light curves of 0.5–2, 2–10, and 0.5–10 keV from Obs. ID 6403520101 in Figure 2. The hardness ratio between 2–10 and 0.5–2 keV is displayed in the bottom panel in Figure 2. The light curve contains three nearly continuous segments, i.e., 0.15–0.25, 1.7–2.05, and 3.5–3.8 hr after the *MAXI* trigger, which are marked as regions I, II, and III, respectively. The count rate of Obs. ID 6403520101 decreased from 1250 to 120 cts/s in 3.6 hr. The count rate in region III is higher than the persistent count rate of about 70 cts/s, therefore the three regions are all considered as part of the burst. Meanwhile, the hardness ratio decreased from 1.3 to 1.1 in region I and maintained at 0.8 and 0.4 in regions II and III, respectively, which indicates the spectral softening during the burst cooling, see Sect. 3.2. We model the 1 s burst light curve in the energy range 0.5–10 keV by an exponential function

$$C(t) = C(t_0)e^{-(t-t_0)/\tau_{LC}} + C_0. \quad (1)$$

The model includes the normalization, $C(t_0)$, the exponential decay time, τ_{LC} , and a constant, C_0 , which represents the asymptotic rate of the burst. We fix the t_0 to the *MAXI* trigger time. The fitted model gives an exponential decay time, $\tau = 0.55 \pm 0.01$ hr, with the reduced- $\chi^2/\text{dof} = 1.35/2306$. We show the best fitted model in the top panel of Figure 2.

We applied the Fast Fourier transform (FFT) method with Leahy normalization (Leahy et al. 1983) to search for the burst oscillation in Obs. ID 6403520101. The power spectra were calculated in the 0.5–3, 3–10, and 0.5–10 keV energy ranges from the cleaned event file, respectively. We adopted a moving window method with the window size T of 8 s, and steps of 1 s. We calculated

¹ <http://maxi.riken.jp/alert/novae/>

² <http://maxi.riken.jp/mxondem/>

the Fourier frequency between 50 and 2000 Hz with an interval of 0.25 Hz in each window (see, e.g. Bilous & Watts 2019; Li et al. 2021). We did not find any prominent signals during the burst in *NICER* observation, and put an upper limit of the fractional root-mean-square amplitude about 5%.

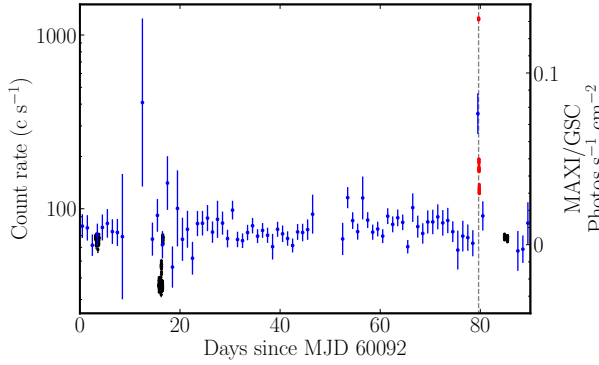


Figure 1. Light curves of 4U 1850-087 from *MAXI* and *NICER* observations. We show the *NICER* light curve (64 s, 0.5–10 keV, black and red points) and the *MAXI* light curve (one day averaged, 2–20 keV, blue points), where the red points represent the *NICER* long X-ray burst’s data. We use the vertical grey dashed line to represent the burst trigger time on MJD 60171.654514 from *MAXI*.

3. SPECTRAL ANALYSIS

We extracted the *NICER* spectra, ancillary response files (ARFs), and response matrix files (RMFs) using `nicer13-spect`, and the 3C50 background spectra were also produced simultaneously (Remillard et al. 2021). We used XSPEC v12.13.0 to analyze the *NICER* spectra in 0.7–10 keV energy band (Arnaud 1996). All bolometric fluxes were estimated in the energy range 0.01–250 keV by using the `cflux` model. The uncertainties were reported at 1 sigma confidence level.

3.1. Persistent Emissions

We fitted the persistent spectra from Obs. ID 6403520102–6403520103 and Obs. ID 6617010101–6617010103 individually. All persistent spectra were grouped with at least 50 counts per channel. The persistent spectra can be well described by a combination of a disk blackbody plus a high-energy Comptonized component (see e.g. Sidoli et al. 2006). We adopted the model `TBabs*(diskbb+nthcomp)` to fit the spectra, where `TBabs` is the interstellar absorption with abundances from Wilms et al. (2000); `diskbb` is a multi-disk blackbody spectrum; `nthcomp` is a thermally Comptonized continuum (Zdziarski et al. 1996; Życki et al. 1999). The model parameters include the asymptotic power law index, Γ , the electron temperature, kT_e , the

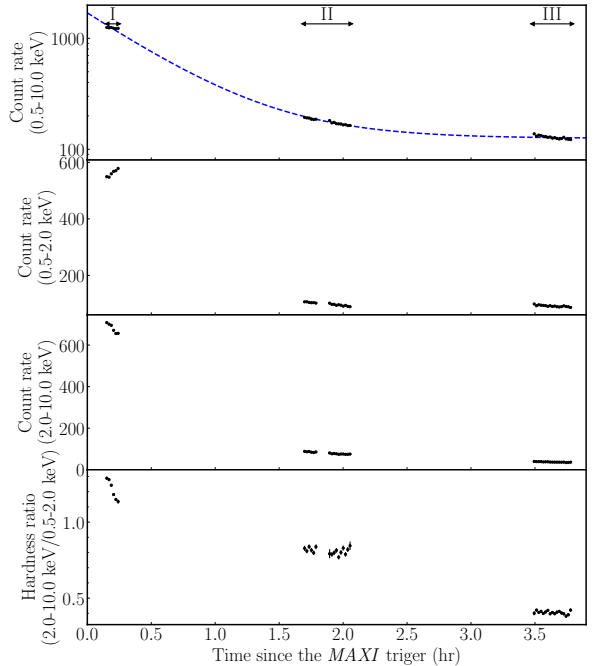


Figure 2. The burst light curves of 4U 1850-087 from *NICER* Obs. ID 6403520101. From top to bottom, we show the 64 s *NICER* burst light curves in the energy range 0.5–10 keV, 0.5–2 keV, and 2–10 keV, and the hardness ratio between 2.0–10 and 0.5–2 keV, respectively. In the top panel, we show the fitted exponential model with the blue dashed line. The time intervals of the regions I, II, and III are represented.

seed photon temperature, $kT_{\text{bb, seed}}$, the input type of seed photons and the normalization for `nthcomp`; the inner disk temperature, kT_{in} , and normalization for `diskbb`; and the equivalent hydrogen column, N_{H} , for `TBabs`. We set the seed photons type from `nthcomp` to 1 and tied the $kT_{\text{bb, seed}}$ to kT_{in} , which means the input seed photons from the accretion disk. Considering the long exposure time for few spectra, the spectra were fitted well from the reduced χ^2 , $\chi^2_{\nu} \sim 0.9 - 1.3$. The best-fitted parameters are listed in Table 1.

The averaged $N_{\text{H}} = 0.606 \pm 0.012 \times 10^{22} \text{ cm}^{-2}$, is consistent with the range of $0.4 - 0.6 \times 10^{22} \text{ cm}^{-2}$ from Sidoli et al. (2006). The disk temperature, radius, and the power-law index of the `nthcomp` component are ~ 0.5 keV, 7 km, and 2.1, respectively. The electron temperature is hard to constraints tightly and the uncertainties are large. These persistent spectra showed quite similar profiles, implying that the persistent emissions did not change significantly. Therefore, we adopted the spec-

trum from Obs. ID 6403520102, which was close to the long X-ray burst, to account for the persistent emission during the burst. We show the best-fitted spectrum and residuals in Figure 3.

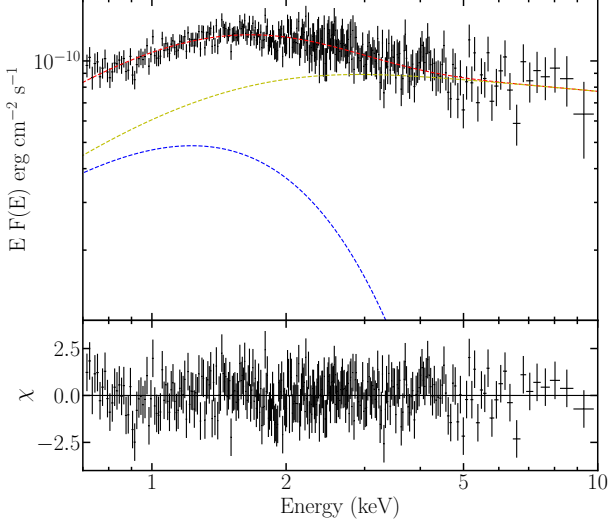


Figure 3. The un-absorbed persistent spectrum and residuals from *NICER* Obs. ID 6403520102 in 0.7–10 keV, which was regarded as the persistent emission during the long X-ray burst. The red, yellow, and blue dashed dots present the model, `nthcomp` component, and `diskbb` component, respectively.

3.2. Time-resolved burst Spectroscopy

We extracted the time-resolved burst spectra with exposure time of 10 s in region I and 100 s in regions II and III from the cleaned event file in Obs. ID 6403520101. We grouped the burst spectra to guarantee that each channel has at least 20 counts by using `grappa`. We first adopted the standard model, `TBabs` \times `bbodyrad`, to fit the burst spectra, where the parameters are the temperature, kT_{bb} , and normalization, $K = R_{\text{bb}}/D_{10 \text{ kpc}}$ where $D_{10 \text{ kpc}}$ is the distance to the source in units of 10 kpc, for `bbodyrad`, and N_{H} for `TBabs`. We fixed the $N_{\text{H}} = 0.6 \times 10^{22} \text{ cm}^{-2}$ and took the persistent spectra from Obs. ID 6403520102 as the burst background. The blackbody model can well describe the burst spectra in regions II and III for χ^2_{ν} close to unity. However, for region I, we obtained the $\chi^2_{\nu} \sim 1.8 - 2.3$, implying poor fits. We show the fitted parameter and χ^2_{ν} as grey stars in Figure 4. The improvements of the fit can be obtained by introducing an extra component from the enhancement of persistent during burst, i.e., the f_a -model (see Sect. 3.2.1), or a reflected emission from the accretion disk, i.e., the reflection model (see Sect. 3.2.2).

3.2.1. Enhanced Persistent Emission

We used the f_a -model, `TBabs` \times (`bbodyrad` + `constant` \times (`nthcomp` + `diskbb`)), to fit the burst spectra, where `constant` accounts for the enhancement of the persistent emission due to the Poynting-Robertson drag (Walker 1992; in’t Zand et al. 2013; Worpel et al. 2013, 2015). Here, we assumed that only the amplitude of the persistent emission was changed if the accretion rate increased during the burst. We adopted the 3c50 spectrum as the instrumental background (Remillard et al. 2022). We fixed N_{H} to the averaged value $0.6 \times 10^{22} \text{ cm}^{-2}$ obtained in Sect. 3.1, the `diskbb` and `nthcomp` parameters to the best-fitted values from the persistent spectra. We show the fitted parameter and χ^2_{ν} as red points in Figure 4. The χ^2_{ν} of f_a -model is around 1.0, which implies the enhancement of the persistent emission can significantly improve the fitted results. The blackbody temperature decreased from $\sim 1.5 \text{ keV}$ during region I to $\sim 0.55 \text{ keV}$ during region III as the burst cooling. As the temperature decreases, the blackbody flux decays from 1×10^{-8} to $1.5 \times 10^{-10} \text{ erg cm}^{-2} \text{ s}^{-1}$. The blackbody radius keeps around 10 km during regions I, II, and III, implying the cooling of the whole NS surface. The enhanced persistent emission was about five times the pre-burst emission in region I and close to the pre-burst level in regions II and III. We can not tell if this burst had experienced a photospheric radius expansion from time-resolved spectroscopy due to the peak of the burst being missed.

3.2.2. The reflection model

The residual of the absorbed blackbody model can also be well described by adding a reflection emission which is illuminated by the long X-ray burst. We use the model `relxillNS` (García et al. 2022) to represent the reflection component (see also Zhao et al. 2022; Lu et al. 2023; Yu et al. 2023). We fitted the burst spectra by `TBabs` \times (`bbodyrad` + `relxillNS`). We fixed all parameters to a constant except the normalization. We tied the input black body temperature, $kT_{\text{bb, in}}$, to the temperature of `bbodyrad`, and set the reflection fraction parameter to -1, which means that this model only represents the reflection emission, and the accretion disk is illuminated by `bbodyrad` photon. We fixed the indices of emissivity, $q_1 = q_2 = 3$, the inner radius of the accretion disk, $R_{\text{in}} = 6R_g$, and the outer radius of the accretion disk, $R_{\text{out}} = 400R_g$, where the R_g is the gravitational radius. Since the spin of 4U 1850–087 is unknown, we assume the spin parameter, a , of the model `relxillNS` to 0.1. We also tried two typical inclination angles, 30° and 60° , to fit the spectra, and found smaller inclination provides slightly better χ^2_{ν} . Therefore, we use 30° as the inclination angle. We let the ionization parameter, $\log \xi$, the

Table 1. Best fitted parameters of all persistent spectra.

<i>NICER</i> (Obs Id)	Exposure (s)	N_{H} (10^{21} cm^{-2})	Γ	kT_e^a (keV)	kT_{in} (keV)	R_{in}^b (km)	F_{per}^c ($10^{-10} \text{ erg cm}^{-2} \text{ s}^{-1}$)	$\chi^2_{\nu}(\text{dof})$
6403520102	647	5.92 ± 0.17	$2.13^{+0.10}_{-0.18}$	$18.46^{+p}_{-17.30}$	0.53 ± 0.04	$6.76^{+1.32}_{-0.63}$	3.86 ± 0.03	0.89(294)
6403520103	1533	5.72 ± 0.12	$2.07^{+0.08}_{-0.09}$	$28.50^{+p}_{-27.50}$	0.56 ± 0.03	$6.08^{+0.38}_{-0.42}$	3.79 ± 0.02	1.05(403)
6617010101	8833	5.98 ± 0.11	$2.13^{+0.04}_{-0.04}$	$31.31^{+p}_{-30.05}$	0.49 ± 0.02	$7.57^{+0.27}_{-0.29}$	3.82 ± 0.02	1.29(643)
6617010102	4492	6.32 ± 0.09	$2.38^{+0.03}_{-0.08}$	$18.31^{+p}_{-17.25}$	0.41 ± 0.03	$7.14^{+1.03}_{-1.79}$	3.75 ± 0.02	1.24(454)
6617010103	3931(p)	6.40 ± 0.12	$2.27^{+0.06}_{-0.08}$	$14.70^{+p}_{-10.67}$	0.40 ± 0.04	$8.71^{+1.21}_{-1.51}$	3.85 ± 0.02	1.13(438)

^a The symbol p means that the poorly constrained electron temperature is pegged at the hard limit.

^b We calculated the inner disk radius by assuming the angle of the disk, $i = 30^\circ$.

^c The unabsorbed bolometric persistent flux in $0.1 - 250 \text{ keV}$.

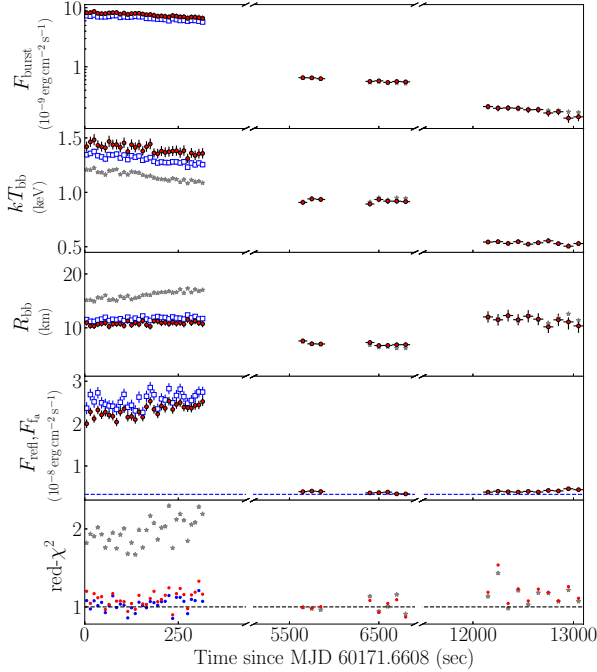


Figure 4. The time-resolved spectroscopy of the long X-ray burst observed by *NICER*. All data points are belonged to part of the long X-ray burst. From top to bottom, we show the bolometric flux of burst, F_{burst} ; the blackbody temperature, kT_{bb} , the blackbody radius, R_{bb} , which were calculated at a distance of 8 kpc; the enhanced persistent flux, F_{fa} , or reflection flux, F_{refl} ; and the goodness of fit per degree of freedom, χ^2_{ν} . The grey star, red dot, and blue square display the results from the blackbody model, the f_a model, and the reflection model, respectively. The blue dashed line represent the persistent emission level. The time zero corresponds to about 0.15 hr after the long burst starts.

iron abundance in the accretion disk in units of solar abundance, A_{Fe} , and the logarithmic density of the accretion disk, $\log n$, free to vary. We found the mean

values of $\log \xi$, A_{Fe} , and $\log n$ are around 2.8, 6, and 16 cm^{-3} during the burst, respectively. Therefore, we fixed these parameters to the corresponding values. We only show the parameters of *relxillNS* in region I, due to the reflection component being insignificant during the cooling tail in regions I and II. The χ^2_{ν} are close to 1 in region I which means the reflection model can also explain the derivations. The best-fitting results are shown in Figure 4 as blue squares. Compared with the f_a -model, the reflection model provides 5% lower blackbody temperatures, 5% higher blackbody radii, and thus 15% lower bolometric fluxes.

3.3. The 1 keV emission line

During the time-resolved burst spectra analysis, we found a faint emission line around 1 keV in region I with an exposure time of 10 s. In order to improve the significance of the emission line, we extracted six spectra in region I with an exposure time of around 50 s for each of them. We used the f_a -model to fit these spectra, same as section 3.2.1. We also extracted longer-duration spectra in regions II and III to find this possible 1 keV feature, but no significant features were found. We also did not find any prominent feature around 1 keV in the persistent spectra. We show the residuals of six spectra in region I, and also the residuals of spectra extracted from regions II and III as comparisons in Figure 5.

We added a **Gaussian** to account for the emission line. The Gaussian parameters of these six spectra are shown in Table 2. We used the *simftest* script in Xspec to evaluate the statistical significance of the **Gaussian** component. For each spectrum, the estimation contains 10^5 sets of simulated data sets. We obtained the probability of the emission line arising by chance less than 1.5×10^{-14} , which means all lines' significance are higher than 7σ . We list the centroid energy in Table 2. By using the reflection model, we also observed this 1 keV feature, but slightly smaller significance.

4. DISCUSSION AND CONCLUSION

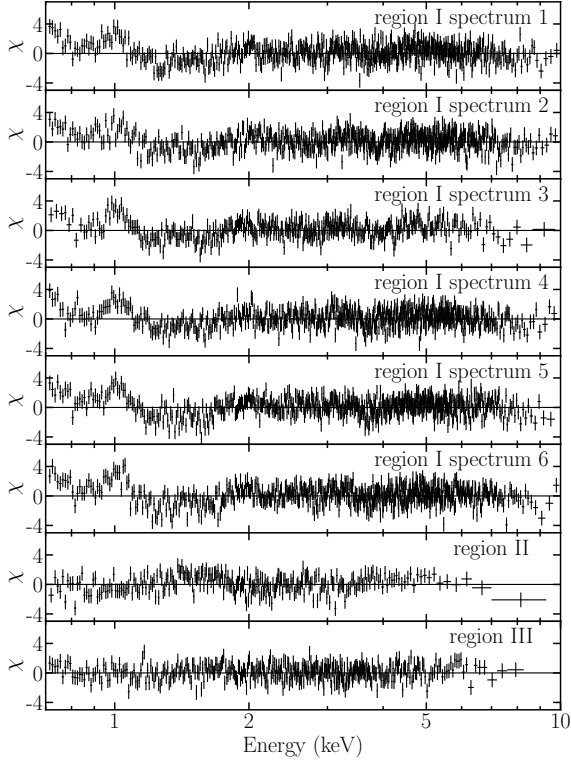


Figure 5. The burst residuals obtained by fitting the f_a -model. We show the error-weighted residuals from the region I-III. The 1 keV emission features are clearly shown in the spectra from region I but not in the spectra from regions II and III.

Table 2. Gaussian line parameters.

Spectra in region I	E_{center} (keV)	Line Norm (photons $\text{cm}^{-2} \text{s}^{-1}$)
1	0.970 ± 0.015	0.034 ± 0.005
2	0.984 ± 0.012	0.037 ± 0.005
3	0.991 ± 0.012	0.032 ± 0.005
4	0.996 ± 0.013	0.030 ± 0.005
5	0.983 ± 0.014	0.035 ± 0.005
6	0.984 ± 0.012	0.037 ± 0.005

4.1. Burst and persistent spectra

In this work, we report the long X-ray burst from 4U 1850–087 observed by *NICER* and *MAXI* observations in 2023. The persistent spectra can be well described by a combination of a multi-color disk blackbody with the inner temperature around 0.5 keV, and a thermally comptonized continuum with the asymptotic power-law photon index of $\Gamma \sim 2.2$, and electron temperature $kT_e \sim 20 - 30$ keV. The persistent spectra are similar across all *NICER* observations, therefore we adopted a

spectrum after the long X-ray burst to represent the persistent emission during burst. We extracted the light curve and identified a long X-ray burst from the Obs. ID 6403520101. To describe the burst evolution, we divide the observation into regions I, II, and III according to the light curve. The spectra from regions II and III were well described by a single blackbody model, but the region I spectra showed clear derivations from the blackbody shape. The results can be improved by adding the enhanced persistent emission due to the Poynting–Robertson drag, the f_a -model, or the reflection emission illuminated by the burst, the reflection model. These two models provided similar burst parameters and χ^2_ν , and are difficult to distinguish.

We use

$$\begin{aligned} \dot{m} &= \frac{L_{\text{per}}(1+z)}{4\pi R_{\text{NS}}^2 (GM_{\text{NS}}/R_{\text{NS}})} \\ &\approx 1.7 \times 10^3 \left(\frac{F_{\text{per}}}{4 \times 10^{-10} \text{ ergs cm}^{-2} \text{ s}^{-1}} \right) \left(\frac{d}{8 \text{ kpc}} \right)^2 \\ &\quad \times \left(\frac{M_{\text{NS}}}{1.4 M_\odot} \right)^{-1} \left(\frac{1+z}{1.31} \right) \left(\frac{R_{\text{NS}}}{10 \text{ km}} \right)^{-1} \text{ g cm}^{-2} \text{ s}^{-1}, \end{aligned} \quad (2)$$

to calculate the local accretion rate, where the F_{per} is the persistent flux, the mass and radius of NS are $M_{\text{NS}} = 1.4 M_\odot$ and $R_{\text{NS}} = 10$ km, the gravitational redshift on NS surface, $z \approx 0.31$, the source distance, $d = 8$ kpc. We obtained $\dot{m} = (1.63 \pm 0.01) \times 10^3 \text{ g cm}^{-2} \text{ s}^{-1}$ for a distance 8 kpc (Paltrinieri et al. 2001). The local Eddington accretion rate is $\dot{m}_{\text{Edd}} = (8.8 \times 10^4) [1.7/(X+1)] \text{ g cm}^{-2} \text{ s}^{-1}$, where X represents the fraction of hydrogen in the accreted material. Considered 4U 1850–087 as an UCXB, $\dot{m} \sim 1\% \dot{m}_{\text{Edd}}$.

4.2. Burst parameters

The decay of the long X-ray burst flux can be well described with the analytic expression by Cumming & Macbeth (2004) and Cumming et al. (2006), leading to constraints on the energy release per unit mass, E_{17} in units of $10^{17} \text{ ergs g}^{-1}$, and the ignition column depth y_{12} in units of $10^{12} \text{ g cm}^{-2}$. We used the trigger time from *MAXI* as the burst peak time which is about 0.15 hr earlier than the first *NICER* observation after the burst. We obtained a poor reduced- $\chi^2/\text{dof} = 2.94/47$ by using all three regions. The burst fluxes in Region III contribute the most significant residuals, which have been also shown in other long bursts (see e.g., Cumming & Macbeth 2004; Cumming et al. 2006). Therefore we only fit the fluxes from Regions I and II. The fit is improved to an acceptable reduced- $\chi^2/\text{dof} = 1.02/37$. We show the fitted f_a -model bolometric flux in Figure 6. We esti-

mated $E_{17} = 0.718 \pm 0.001$, $y_{12} = 0.035 \pm 0.001$ and the burst peak flux $F_{\text{peak}} = 1.88 \pm 0.07 \times 10^{-8} \text{ erg cm}^{-2} \text{ s}^{-1}$. The burst peak flux is less than the Eddington flux, that is $F_{\text{Edd}} \approx 3.8 \times 10^{-8} \text{ erg cm}^{-2} \text{ s}^{-1}$ in hydrogen poor environment, which indicates the photospheric radius expansion may not appear in the burst.

We then use

$$f_b = \frac{4\pi y_{\text{ign}} R_{\text{NS}}^2 Q_{\text{nuc}}}{4\pi d^2 (1+z)}, \quad (3)$$

to calculate the burst fluence from the estimated ignition column depth y_{ign} , where $Q_{\text{nuc}} \approx 1.31 \text{ MeV nucleon}^{-1}$ for a given hydrogen fraction of $X = 0$ (Goodwin et al. 2019). We obtained the burst fluence $f_b = 5.3 \pm 0.2 \times 10^{-5} \text{ erg cm}^{-2}$. We then calculated the burst decay time $\tau = f_b / F_{\text{peak}} \approx 0.78 \pm 0.04 \text{ hr}$, which is higher than the exponential decay time 0.55 hr fitted from the light curve. All the burst parameters are reported in Table 3. We added two intermediate-duration bursts' parameters of 4U 1850-087 from *MAXI* and *Swift* data in Table 3 as a comparison (Serino et al. 2016; in't Zand et al. 2014). The burst fluence and total released energy are rescaled to a distance of 8 kpc. Compared to the other two bursts, the burst has a smaller peak flux, a similar total burst emitted energy, and a longest burst decay time. The predicted recurrence time is obtained via the relation $\Delta t_{\text{rec}} = y(1+z)/\dot{m}$. We found that the observed recurrence time, ΔT_{rec} , of the long X-ray burst observed in 2015, which is higher than the predicted value. The discrepancy may be caused by the not well calibrated flux from *MAXI*, i.e., the burst peak flux is two times higher than the Eddington limit. The predicted recurrence time of the long X-ray in our work, 0.87 yr, is lower than the observed value, 7.76 yr, which means that some long or normal X-ray bursts were likely missed during 2015-2023 due to poorly coverage of the observations.

4.3. Burst fuel

The decay time of the burst from 4U 1850-087 on August 15, 2023, $\tau \sim 0.78 \text{ h}$, which is within the longest intermediate-duration bursts and shortest superbursts. The burst decay time in some longest intermediate-duration bursts are 0.8 hr from SAX J1712.6-3739 (in't Zand et al. 2019), and 0.71 hr from 4U 1850-087 (see Table 3, Serino et al. 2016). The burst duration of several shortest superbursts were 0.7 and 1.0 hr from GX 17+2, 1.2 hr from Ser X-1, and 2.1 hr from 4U 0614+091 (Keek et al. 2010). The accretion rate of GX 17+2 and Ser X-1 are $> 20\% \dot{m}_{\text{Edd}}$, of 4U 0614+091 are $< 1\% \dot{m}_{\text{Edd}}$. The donor star of 4U 1850-08 is a white dwarf or helium star, which means the accretion mat-

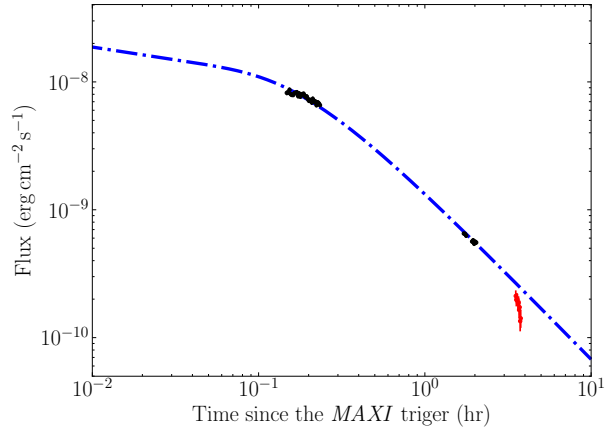


Figure 6. The burst flux fitted by the model which proposed in Cumming & Macbeth (2004) during the burst decay. The burst flux was estimated from the f_a model. The black points represent the data in regions I and II. The red points represent the region III data, which were excluded from the fit. We use the trigger time in *MAXI* as the burst peak time.

ter includes a large pile of helium. At a low accretion rate $\sim 1\% \dot{m}_{\text{Edd}}$, the carbon is difficult to accumulate (Cumming et al. 2006). Considering the burst decay time is less than the superburst with a low accretion rate from 4U 0614+091 and the calculated recurrence time consistent with the observed recurrence time between the other two intermediate-duration bursts from 4U 1850-087 (see Table 3), we propose that this burst is the longest intermediate-duration burst like other long X-ray bursts observed in 4U 1850-08 (in't Zand et al. 2014; Serino et al. 2016). We also calculated the ratio of the total persistent flux between two bursts to the total energy emitted from burst $\alpha = (F_{\text{pers}} \times \Delta T_{\text{rec}}) / f_b \sim 117$, which the shortest observed recurrence time of 0.51 hr in Table 3 is used. When we assume all accreted fuel burned during the burst, we calculated the theoretical $\alpha = 44 M_{\text{NS}} R_{\text{NS}}^{-1} (Q_{\text{nuc}} / 4.4 \text{ MeV/nucleon})^{-1} \approx 121$ (Falanga et al. 2008). The calculated α from measurable quantities is close to a pure helium burst, which is also support the burst as an intermediate-duration burst.

4.4. The origin of the 1 keV emission line

We found an emission feature near 1 keV in the burst spectrum, which can be improved by adding a Gaussian component. This line can only be detected in region I, but not in regions II and III, and the persistent spectra, which suggests that this line does not come from the instrumental effect. By using the tool *simfest*, we estimated the significance of the emission line, $> 7\sigma$, which proves that it is not caused by random fluctua-

Table 3. The parameters of long X-ray bursts from 4U 1850–087.

Burst date	F_{peak} (10^{-8} erg cm $^{-2}$ s $^{-1}$)	E_b (10^{41} erg)	f_b (10^{-5} erg cm $^{-2}$)	τ (hr)	$\Delta t_{\text{rec}} \equiv y(1+z)/\dot{m}$ (year)	ΔT_{rec}^a (year)
2014-03-10 ^b	10.7 \pm 0.9	7.9 \pm 0.7	10.3 \pm 0.9	0.27	1.70	-
2015-05-09 ^b	7.8 \pm 0.5	14.8 \pm 0.9	19.3 \pm 1.2	0.71	3.18	1.16
2015-11-11 ^c	-	-	-	-	-	0.51
2023-08-15	1.88 \pm 0.07	4.1 \pm 0.2	5.3 \pm 0.2	0.78 \pm 0.04	0.87 \pm 0.03	7.76

^a T_{rec} means the time interval between the current burst and the previous one. T_{rec} only presents the upper limit of burst recurrence time due to the data gap of observations.

^b The data of bursts in 2014 and 2015 were taken simply from in't Zand et al. (2014); Serino et al. (2016). Note that the distance of 8 kpc rather than 6.9 kpc was adopted to recalculate E_b and f_b .

^c The trigger time of bursts were taken from the *MAXI* novae webpage.

tions. Therefore, we propose that this line is caused by an astrophysical origin.

A weaker 1 keV emission line was also detected in an intermediate duration burst of 4U 1850–087 by *Swift* (see in't Zand 2017). The similar emission line have also been detected in IGR J17062–6143 (Bult et al. 2021a), SAX J1808.4–3658 (Bult et al. 2019), and 4U 1820–30 (Strohmayer et al. 2019). The line in IGR J17062–6143 has been explained by the Fe L shell transitions or Ly α transition of Ne X at 1.022 keV in the accretion disk (Keek et al. 2017; Degenaar et al. 2013) or the emit from photoionized plasma illuminated by a blackbody continuum (Bult et al. 2021a). The 1 keV emission line in 4U 1820–30 was detected in an PRE burst, which were

possibly produced in the PRE wind (Strohmayer et al. 2019). Considering we did not find the photosphere expansion in time-resolved spectra, the 1 keV emission line is likely produced in the accretion disk.

- 1 This work was supported by the Major Science and
- 2 Technology Program of Xinjiang Uygur Autonomous
- 3 Region (No. 2022A03013-3). Z.S.L. and Y.Y.P. were
- 4 supported by National Natural Science Foundation of
- 5 China (12273030, 12103042). This work made use of
- 6 data from the High Energy Astrophysics Science Archive
- 7 Research Center (HEASARC), provided by NASA's
- 8 Goddard Space Flight Center.

REFERENCES

- Alizai, K., Chenevez, J., Cumming, A., et al. 2023, MNRAS, 521, 3608, doi: [10.1093/mnras/stad374](https://doi.org/10.1093/mnras/stad374)
- Arnaud, K. A. 1996, in Astronomical Society of the Pacific Conference Series, Vol. 101, Astronomical Data Analysis Software and Systems V, ed. G. H. Jacoby & J. Barnes, 17
- Ballantyne, D. R., & Strohmayer, T. E. 2004, ApJL, 602, L105, doi: [10.1086/382703](https://doi.org/10.1086/382703)
- Bilous, A. V., & Watts, A. L. 2019, ApJS, 245, 19, doi: [10.3847/1538-4365/ab2fe1](https://doi.org/10.3847/1538-4365/ab2fe1)
- Bult, P., Jaisawal, G. K., Güver, T., et al. 2019, ApJL, 885, L1, doi: [10.3847/2041-8213/ab4ae1](https://doi.org/10.3847/2041-8213/ab4ae1)
- Bult, P., Altamirano, D., Arzoumanian, Z., et al. 2021a, ApJ, 920, 59, doi: [10.3847/1538-4357/ac18c4](https://doi.org/10.3847/1538-4357/ac18c4)
- . 2021b, ApJ, 907, 79, doi: [10.3847/1538-4357/abd54b](https://doi.org/10.3847/1538-4357/abd54b)
- Cumming, A., & Bildsten, L. 2001, ApJL, 559, L127, doi: [10.1086/323937](https://doi.org/10.1086/323937)
- Cumming, A., & Macbeth, J. 2004, ApJL, 603, L37, doi: [10.1086/382873](https://doi.org/10.1086/382873)
- Cumming, A., Macbeth, J., in 't Zand, J. J. M., & Page, D. 2006, ApJ, 646, 429, doi: [10.1086/504698](https://doi.org/10.1086/504698)
- Degenaar, N., Miller, J. M., Wijnands, R., Altamirano, D., & Fabian, A. C. 2013, The Astrophysical Journal, 767, L37, doi: [10.1088/2041-8205/767/2/L37](https://doi.org/10.1088/2041-8205/767/2/L37)
- Falanga, M., Chenevez, J., Cumming, A., et al. 2008, A&A, 484, 43, doi: [10.1051/0004-6361:20078982](https://doi.org/10.1051/0004-6361:20078982)
- Galloway, D. K., & Keek, L. 2021, Astrophysics and Space Science Library, 461, 209, doi: [10.1007/978-3-662-62110-3_5](https://doi.org/10.1007/978-3-662-62110-3_5)
- Galloway, D. K., Munro, M. P., Hartman, J. M., Psaltis, D., & Chakrabarty, D. 2008, The Astrophysical Journal Supplement Series, 179, 360
- Galloway, D. K., in't Zand, J., Chenevez, J., et al. 2020, ApJS, 249, 32, doi: [10.3847/1538-4365/ab9f2e](https://doi.org/10.3847/1538-4365/ab9f2e)
- García, J. A., Dauser, T., Ludlam, R., et al. 2022, ApJ, 926, 13, doi: [10.3847/1538-4357/ac3cb7](https://doi.org/10.3847/1538-4357/ac3cb7)
- Goodwin, A. J., Heger, A., & Galloway, D. K. 2019, ApJ, 870, 64, doi: [10.3847/1538-4357/aaced2](https://doi.org/10.3847/1538-4357/aaced2)

- Homer, L., Charles, P. A., Naylor, T., et al. 1996, MNRAS, 282, L37, doi: [10.1093/mnras/282.3.L37](https://doi.org/10.1093/mnras/282.3.L37)
- in't Zand, J. 2017, in 7 years of MAXI: monitoring X-ray Transients, ed. M. Serino, M. Shidatsu, W. Iwakiri, & T. Mihara, 121. <https://arxiv.org/abs/1702.04899>
- in't Zand, J., Linares, M., & Markwardt, C. 2014, The Astronomer's Telegram, 5972, 1
- in't Zand, J. J. M., Cumming, A., van der Sluys, M. V., Verbunt, F., & Pols, O. R. 2005, A&A, 441, 675, doi: [10.1051/0004-6361:20053002](https://doi.org/10.1051/0004-6361:20053002)
- in't Zand, J. J. M., Kries, M. J. W., Palmer, D. M., & Degenaar, N. 2019, A&A, 621, A53, doi: [10.1051/0004-6361/201834270](https://doi.org/10.1051/0004-6361/201834270)
- in't Zand, J. J. M., Galloway, D. K., Marshall, H. L., et al. 2013, A&A, 553, A83, doi: [10.1051/0004-6361/201321056](https://doi.org/10.1051/0004-6361/201321056)
- Keek, L., Ballantyne, D. R., Kuulkers, E., & Strohmayer, T. E. 2014, ApJL, 797, L23, doi: [10.1088/2041-8205/797/2/L23](https://doi.org/10.1088/2041-8205/797/2/L23)
- Keek, L., Galloway, D. K., in't Zand, J. J. M., & Heger, A. 2010, ApJ, 718, 292, doi: [10.1088/0004-637X/718/1/292](https://doi.org/10.1088/0004-637X/718/1/292)
- Keek, L., Heger, A., & in't Zand, J. J. M. 2012, ApJ, 752, 150, doi: [10.1088/0004-637X/752/2/150](https://doi.org/10.1088/0004-637X/752/2/150)
- Keek, L., Iwakiri, W., Serino, M., et al. 2017, ApJ, 836, 111, doi: [10.3847/1538-4357/836/1/111](https://doi.org/10.3847/1538-4357/836/1/111)
- Kuulkers, E., in't Zand, J. J. M., Atteia, J. L., et al. 2010, A&A, 514, A65, doi: [10.1051/0004-6361/200913210](https://doi.org/10.1051/0004-6361/200913210)
- Lasota, J.-P. 2001, NewAR, 45, 449, doi: [10.1016/S1387-6473\(01\)00112-9](https://doi.org/10.1016/S1387-6473(01)00112-9)
- Leahy, D. A., Darbro, W., Elsner, R. F., et al. 1983, ApJ, 266, 160, doi: [10.1086/160766](https://doi.org/10.1086/160766)
- Lewin, W. H. G., van Paradijs, J., & Taam, R. E. 1993, SSRv, 62, 223, doi: [10.1007/BF00196124](https://doi.org/10.1007/BF00196124)
- Li, Z., Pan, Y., & Falanga, M. 2021, ApJ, 920, 35, doi: [10.3847/1538-4357/ac1f15](https://doi.org/10.3847/1538-4357/ac1f15)
- Lu, Y., Li, Z., Pan, Y., et al. 2023, A&A, 670, A87, doi: [10.1051/0004-6361/202244984](https://doi.org/10.1051/0004-6361/202244984)
- Paltrinieri, B., Ferraro, F. R., Paresce, F., & De Marchi, G. 2001, AJ, 121, 3114, doi: [10.1086/321069](https://doi.org/10.1086/321069)
- Remillard, R. A., Loewenstein, M., Steiner, J. F., et al. 2021, arXiv e-prints, arXiv:2105.09901. <https://arxiv.org/abs/2105.09901>
- . 2022, AJ, 163, 130, doi: [10.3847/1538-3881/ac4ae6](https://doi.org/10.3847/1538-3881/ac4ae6)
- Serino, M., Iwakiri, W., Tamagawa, T., et al. 2016, PASJ, 68, 95, doi: [10.1093/pasj/psw086](https://doi.org/10.1093/pasj/psw086)
- Sidoli, L., La Palombara, N., Oosterbroek, T., & Parmar, A. N. 2005, A&A, 443, 223, doi: [10.1051/0004-6361:20053438](https://doi.org/10.1051/0004-6361:20053438)
- Sidoli, L., Paizis, A., Bazzano, A., & Mereghetti, S. 2006, A&A, 460, 229, doi: [10.1051/0004-6361:20065759](https://doi.org/10.1051/0004-6361:20065759)
- Strohmayer, T., & Bildsten, L. 2006, in Compact stellar X-ray sources, Cambridge Astrophysics Series, No. 39, ed. W. Lewin & M. van der Klis (Cambridge: Cambridge University Press), 113–156
- Strohmayer, T. E., & Brown, E. F. 2002, ApJ, 566, 1045, doi: [10.1086/338337](https://doi.org/10.1086/338337)
- Strohmayer, T. E., Altamirano, D., Arzoumanian, Z., et al. 2019, ApJL, 878, L27, doi: [10.3847/2041-8213/ab25eb](https://doi.org/10.3847/2041-8213/ab25eb)
- Swank, J. H., Becker, R. H., Pravdo, S. H., Saba, J. R., & Serlemitsos, P. J. 1976, IAUC, 3010, 1
- Tremou, E., Strader, J., Chomiuk, L., et al. 2018, ApJ, 862, 16, doi: [10.3847/1538-4357/aac9b9](https://doi.org/10.3847/1538-4357/aac9b9)
- Walker, M. A. 1992, ApJ, 385, 642, doi: [10.1086/170969](https://doi.org/10.1086/170969)
- Wilms, J., Allen, A., & McCray, R. 2000, The Astrophysical Journal, 542, 914, doi: [10.1086/317016](https://doi.org/10.1086/317016)
- Worpel, H., Galloway, D. K., & Price, D. J. 2013, ApJ, 772, 94, doi: [10.1088/0004-637X/772/2/94](https://doi.org/10.1088/0004-637X/772/2/94)
- . 2015, ApJ, 801, 60, doi: [10.1088/0004-637X/801/1/60](https://doi.org/10.1088/0004-637X/801/1/60)
- Yu, W., Li, Z., Lu, Y., et al. 2023, arXiv e-prints, arXiv:2312.16420, doi: [10.48550/arXiv.2312.16420](https://doi.org/10.48550/arXiv.2312.16420)
- Zdziarski, A. A., Johnson, W. N., & Magdziarz, P. 1996, MNRAS, 283, 193, doi: [10.1093/mnras/283.1.193](https://doi.org/10.1093/mnras/283.1.193)
- Zhao, G., Li, Z., Pan, Y., et al. 2022, A&A, 660, A31, doi: [10.1051/0004-6361/202142801](https://doi.org/10.1051/0004-6361/202142801)
- Życki, P. T., Done, C., & Smith, D. A. 1999, MNRAS, 309, 561, doi: [10.1046/j.1365-8711.1999.02885.x](https://doi.org/10.1046/j.1365-8711.1999.02885.x)